IJARSCT
International Journal of Advanced Research in Science, Communication and Technology
International Open-Access, Double-Blind, Peer-Reviewed, Refereed, Multidisciplinary Online Journal
ISSN: 2581-9429
Volume 5, Issue 8, April 2025
Impact Factor: 7.67

Structural and Optical Study of Lead Doping on Cobalt Ferrite Nanoparticles Synthesized via Sol-Gel Autocombution Method

AltafIsuf Fakir[1], Masira Abdul Jalil Pangarkar[2], Fatima Nasir Surve[2]
Anjuman Islam Janjira Degree College of Science, Murud Janjira[1-2]

Abstract: *Lead (Pb^{2+}) substituted cobalt ferrite ($Co_{1-x}Pb_xFe_2O_4$, x = 0.1–0.5) nanoparticles were synthesized via the sol-gel autocombustion method to investigate the impact of Pb^{2+} concentration on structural and optical properties. X-ray diffraction (XRD) confirmed phase purity, with an increasing lattice parameter due to the larger ionic radius of Pb^{2+}. UV-Visible spectroscopy revealed an absorption edge shift (690–703 nm), and band gap values were determined using both absorption edge and Tauc's plot methods. The band gap decreased up to x = 0.3 due to impurity band formation and grain size effects but increased at x > 0.3, attributed to the Burstein–Moss effect. The findings highlight the tunability of CoFe□O□ properties through Pb^{2+} substitution, making them promising for optoelectronic applications.*

Keywords: Nanoparticles, Cobalt Ferrite, Sol-Gel Method, Optical Properties

I. INTRODUCTION

Cobalt ferrites have attracted considerable attention due to their extensive industrial and research applications, stemming from their outstanding magnetic, electrical, and structural properties. They belong to the ferrite group, which offers tunable characteristics through the substitution of various cations such as Zn^{2+}, Ni^{2+}, Cu^{2+}, and Pb^{2+}. This cationic substitution allows for modifications in the material's properties, enhancing its suitability for diverse applications [1]. These include high-frequency electronic devices, memory cores, high-density data storage, and biomedical applications such as ferrofluids, magnetic drug delivery, and hyperthermia-based cancer treatment [2].Cobalt ferrite ($CoFe_2O_4$) exhibits an inverse spinel structure, where Co^{2+} ions primarily occupy octahedral (B) sites, while Fe^{3+} ions are distributed between tetrahedral (A) and octahedral (B) sites. The incorporation of Pb^{2+} into $CoFe_2O_4$ can lead to structural distortions depending on precursor concentration, as $PbFe_2O_4$ typically forms a spinel structure with Pb^{2+} in tetrahedral positions and Fe^{3+} in octahedral positions. The sol-gel technique stands out among synthesis methods due to its ability to produce ultrafine ferrite powders with high compositional homogeneity at relatively low temperatures [3].It has been found that in DC electrical resistivity study of the samples was found to be increases with increasing Pb2+from x= 0.1 to x = 0.5. That means the conductivity decreases with increasing concentration of lead but it increases with increasing voltage[4].

In this study, lead (Pb^{2+})-substituted cobalt ferrite ($Co_{1-x}Pb_xFe_2O_4$, where x = 0.1 to 0.5) nanoparticles are synthesized using the sol-gel method. The research focuses on analyzing the impact of Pb^{2+} ion concentration on the structural and optical properties of the synthesized nanoparticles. The influence of lead substitution on crystallinity and band gap energy is examined to understand its role in tuning the material's functional characteristics for potential applications in electronics and biomedical fields.

II. SYNTHESIS METHOD

The sol-gel synthesis method was employed to prepare Pb^{2+}-substituted cobalt ferrite ($Co_{1-x}Pb_xFe_2O_4$), where x = 0.1, 0.2, 0.3, 0.4, and 0.5. The stoichiometric amounts of ferric nitrate ($Fe(NO_3)_3$), lead nitrate ($Pb(NO_3)_2$), and cobalt nitrate ($Co(NO_3)_2 \cdot 6H_2O$) were dissolved in 100 ml of distilled water under continuous magnetic stirring. To facilitate the removal of Co^{2+}, Pb^{2+}, and Fe^{3+} ions, citric acid ($C_6H_8O_7$) was added to the metal nitrate solution while maintaining a molar ratio of 1:3 between citric acid and the total metal nitrates. a controlled amount of ammonia was added

DOI: 10.48175/IJARSCT-25501

IJARSCT
International Journal of Advanced Research in Science, Communication and Technology
International Open-Access, Double-Blind, Peer-Reviewed, Refereed, Multidisciplinary Online Journal
ISSN: 2581-9429
Volume 5, Issue 8, April 2025
Impact Factor: 7.67

dropwise to stabilize the nitrate-citrate solution and adjust the pH to approximately 7. The solution underwent vigorous stirring and was heated at 100°C for one hour, allowing it to evaporate and transform into a gel. The gel was subsequently heated to 150°C to initiate auto-combustion. The resulting powder was finely ground using an agate mortar and subjected to sintering at 600°C for four hours to obtain the final nanoferrite particles.

III. CHARACTERIZATION TECHNIQUES

Pb^{2+} substituted $CoFe_2O_4$ ferrites were structurally analyzed using X-ray diffraction (XRD) to investigate their phase composition. The XRD patterns were recorded with Cu-Kα radiation(λ = 1.54182 Å) in the 2θ range of 20° to 80° with a step size of 0.01° and a time per step of 2s.UV-Visible spectroscopy was employed to examine the optical and electronic properties of the synthesized ferrites. The energy band gap (Eg), a key parameter influencing optoelectronic applications, was determined using the absorption edge method (E=hc/λ), where h is Planck's constant, c is the speed of light, and λ is the absorption edge wavelength.The band gap energy was further analyzed using Tauc's relation:

$$\alpha h\upsilon = B(h\upsilon - Eg)^n$$

where α is the absorption coefficient, B is a proportionality constant, h is Planck's constant, ν is the photon energy, and n is 0.5 for direct transitions and 2 for indirect transitions. The optical band gap for direct transitions was obtained by extrapolating the linear region of a $(\alpha h\nu)^2$vs. (hν) plot.

IV. RESULTS AND DISCUSSION

1) X-Ray Diffraction:

Fig. 1(a) presents the XRD patterns of Pb-doped $CoFe_2O_4$ samples (x = 0.1–0.5), confirming phase purity due to the absence of additional peaks. The diffraction peaks match the JCPDS Card No. 22-1086 for $CoFe_2O_4$. The average grain size, calculated using the Debye-Scherrer formula, ranged from 34.5 to 54.5 nm, though variations in particle size were observed with increasing Pb^{2+} content [5].

The lattice parameter a, determined from XRD data, ranged from 8.3877 to 8.4108 Å, increasing with Pb^{2+} substitution due to the larger ionic radius of Pb^{2+} (1.19 Å) compared to Co^{2+} (0.7 Å)[6]. Fig. 1(b) illustrates the shift in diffraction angle (2θ) with Pb^{2+} content. Lower angle shifts (x = 0.3–0.5) indicate compressive strain with increasing interplanar spacing (d), while higher angle shifts (x = 0.2) suggest tensile strain and reduced interplanar spacing [7].

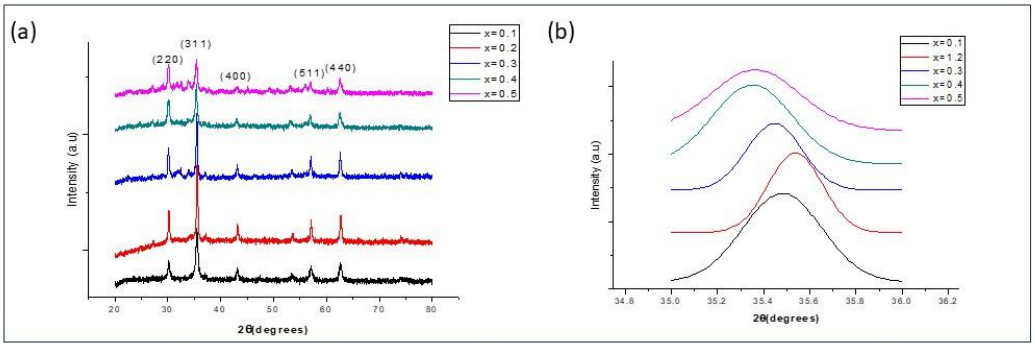

Figure 1*(a) XRD patterns of Pb^{2+} substituted $CoFe_2O_4$ samples at Pb^{2+} concentrations of x=0.1, 0.2, 0.3, 0.4, and 0.5.(b) Graph of shift in diffraction angle (2θ) with increasing Pb^{2+} concentration.*

2) UV-Visible spectroscopy

UV-Visible spectroscopy is a widely used technique for analyzing the optical properties of materials, particularly in determining their energy band gap (Eg), which plays a crucial role in semiconductor applications, including optoelectronic devices[8]. The UV-Vis absorbance spectra of Pb^{2+} doped $CoFe_2O_4$ samples (x = 0.1, 0.2, 0.3, 0.4, 0.5) are shown in Figure 2, recorded at room temperature. All samples exhibit an absorption edge within the wavelength

IJARSCT
International Journal of Advanced Research in Science, Communication and Technology
International Open-Access, Double-Blind, Peer-Reviewed, Refereed, Multidisciplinary Online Journal
ISSN: 2581-9429
Volume 5, Issue 8, April 2025
Impact Factor: 7.67

range of 690 nm to 703 nm.The energy band gap (Eg) can be estimated using the absorption edge wavelength (λ) and the relation:

$E=hc/\lambda$

where h is Planck's constant, c is the speed of light, and λ is the absorption edge wavelength. A slight variation in the band gap values with increasing Pb^{2+} concentration suggests changes in electronic structure due to Pb^{2+} incorporation. The shift in the absorption edge indicates a modification in the material's optical response, which may influence its potential applications in photonic and optoelectronic devices [9].

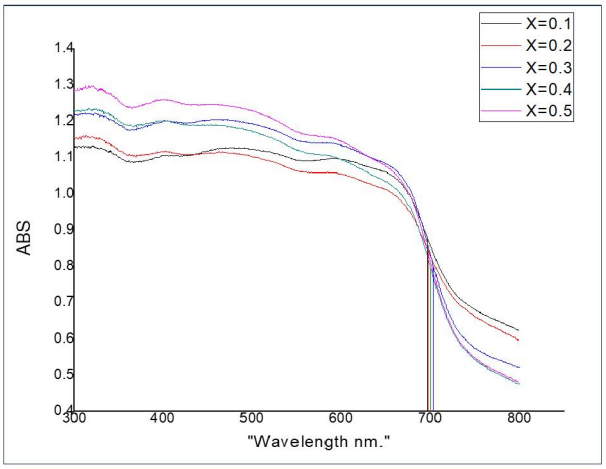

Figure 2 *UV-Visible absorption spectra of Pb^{2+} doped $CoFe_2O_4$ samples with Pb^{2+} concentrations of x = 0.1, 0.2, 0.3, 0.4, and 0.5.*

Figure 3 presents the Tauc plot for Pb^{2+} doped $CoFe_2O_4$ with varying Pb^{2+} concentrations (x = 0.1, 0.2, 0.3, 0.4, 0.5). The optical band gap values, determined using the Tauc relation, closely match those obtained from the absorption edge method. A notable trend is observed where the band gap initially decreases up to x = 0.3 and then increases for higher Pb^{2+} concentrations, as depicted in **Figure 5.**

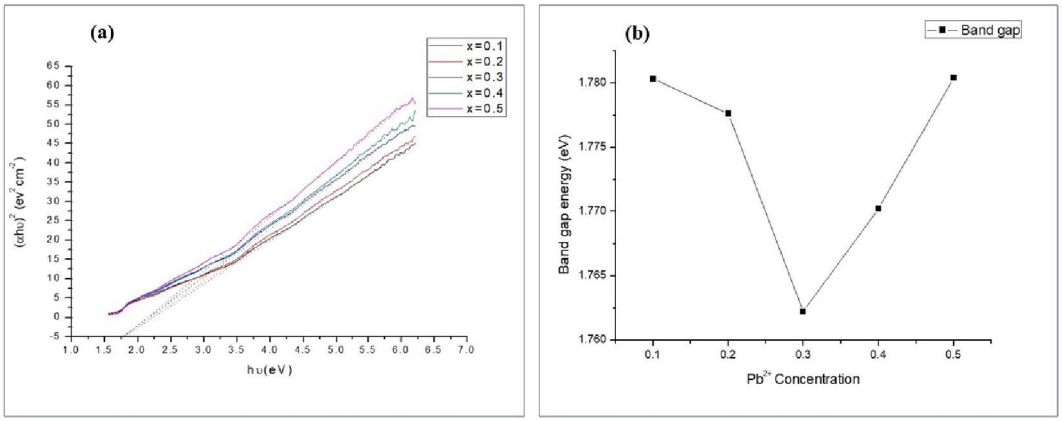

Figure 3*(a) Tauc plot for Pb^{2+} doped $CoFe_2O_4$ samples with Pb^{2+} concentrations of x = 0.1, 0.2, 0.3, 0.4, and 0.5. (b) Variation in optical band gap energy as a function of Pb^{2+} concentration.*

The decrease in band gap up to x = 0.3 can be attributed to the formation of impurity bands due to Pb^{2+} substitution for Co^{2+}. At lower dopant concentrations, these impurity bands introduce states within the band gap, effectively reducing the energy gap. As Pb^{2+} content increases, the impurity bands broaden and begin to overlap, further lowering the band gap [10]. Additionally, this reduction may also be linked to an increase in grain size, as larger particles lead to a narrowing of energy bands due to increased orbital overlap.Beyond x = 0.3, the band gap increases, which can be explained by the Burstein–Moss effect [11]. As more Pb^{2+} is incorporated, the conduction band becomes progressively

IJARSCT
International Journal of Advanced Research in Science, Communication and Technology
International Open-Access, Double-Blind, Peer-Reviewed, Refereed, Multidisciplinary Online Journal
ISSN: 2581-9429
Volume 5, Issue 8, April 2025
Impact Factor: 7.67

occupied, pushing the Fermi level higher and shifting the absorption edge to higher energies. This results in an apparent increase in the band gap, given by the sum of the actual band gap and the Burstein–Moss shift. The increase in band gap at $x > 0.3$ may also be associated with a decrease in grain size, as smaller particles exhibit quantum confinement effects, leading to band gap widening [12].The UV-Vis absorption results align well with the XRD findings, confirming the influence of Pb^{2+} substitution on the structural and optical properties of $CoFe_2O_4$.

V. CONCLUSION

The sol-gel synthesis method successfully produced Pb^{2+} doped cobalt ferrite ($Co_{1-x}Pb_xFe_2O_4$) nanoparticles with varying Pb^{2+} concentrations (x=0.1 - 0.5). Structural analysis via XRD confirmed the phase purity of the synthesized ferrites, with lattice parameters increasing due to the larger ionic radius of Pb^{2+} compared to Co^{2+}. The average grain size ranged from 34.5 to 54.5 nm, with shifts in diffraction angles indicating changes in interplanar spacing and strain effects. UV-Visible spectroscopy revealed that the optical band gap initially decreased with Pb^{2+} substitution up to x = 0.3, attributed to impurity band formation and increased grain size, and then increased at higher Pb^{2+} concentrations due to the Burstein Moss effect and potential quantum confinement. These findings demonstrate that Pb^{2+} incorporation significantly influences the structural and optical properties of $CoFe_2O_4$, making it a promising candidate for optoelectronic applications. The correlation between XRD and UV-Visible results features the tunability of the material's properties through controlled doping, offering potential for personalized applications in photonic and semiconductor devices.

REFERENCES

[1] D. S. Mathew and R. S. Juang, "An overview of the structure and magnetism of spinel ferrite nanoparticles and their synthesis in microemulsions," *Chem. Eng. J.*, vol. 129, no. 1–3, pp. 51–65, May 2007, doi:10.1016/J.CEJ.2006.11.001.

[2] C. Moya, M. D. P. Morales, X. Batlle, and A. Labarta, "Tuning the magnetic properties of Co-ferrite nanoparticles through the 1,2-hexadecanediol concentration in the reaction mixture," Phys. Chem. Chem Phys., vol. 17, no. 19, pp. 13143–13149, 2015, doi: 10.1039/c5cp01052g.

[3] Shirsath, Sagar& Wang, Danyang&Jadhav, Swati & Mane, Maheshkumar& Li, Sean. (2018). Ferrites Obtained by Sol-Gel Method. 10.1007/978-3-319-32101-1_125.

[4] Fakir, A. I., Hukebardar, M. M., & More, A. J. (2023). *Effect of Pb 2 + Doping on the Electrical Properties of Cobalt Ferrite Nano Particles Prepared via Sol- Gel Route*. *4*(3), 8–12.

[5] M. Lakshmi, K. V. Kumar, K. Thyagarajan, M. Lakshmi, K. V. Kumar, and K. Thyagarajan, "Structural and Magnetic Properties of Cr-Co Nanoferrite Particles," Adv. Nanoparticles, vol. 5, no. 1, pp. 103–113, Feb. 2016, doi:10.4236/ANP.2016.51012.

[6] Kumar, R., &Kar, M. (2016). Correlation between lattice strain and magnetic behavior in non-magnetic Ca substituted nano-crystalline cobalt ferrite. Ceramics International, 42(6), 6640–6647. https://doi.org/10.1016/J.CERAMINT.2016.01.007

[7] Örnek, C., &Engelberg, D. L. (2016). An experimental investigation into strain and stress partitioning of duplex stainless steel using digital image correlation, X-ray diffraction and scanning Kelvin probe force microscopy. Journal of Strain Analysis for Engineering Design, 51(3),207–219. https://doi.org/10.1177/0309324716631669/ASSET/IMAGES/LARGE/10.1177_0309324716631669-FIG14.JPEG

[8] Soonmin, H. (2022). Investigation of Optical Properties of Thin Films by Means of UV-visible Spectrophotometer: A Review. New Frontiers in Physical Science Research Vol. 5, 66–82. https://doi.org/10.9734/BPI/NFPSR/V5/4498E

[9] Sobola, D., Fawaeer, S. H., Kočková, P., Schubert, R., Dallaev, R., &Trčka, T. (2024). Optical Properties of Yttrium Ferrite Films Prepared by Pulse Laser Deposition. Coatings, 14(11). https://doi.org/10.3390/COATINGS14111464/S1

[10] Pramanik, Md. B., al Rakib, Md. A., Siddik, Md. A., &Bhuiyan, S. (2024). Doping Effects and Relationship between Energy Band Gaps, Impact of Ionization Coefficient and Light Absorption Coefficient in Semiconductors.

IJARSCT
International Journal of Advanced Research in Science, Communication and Technology
International Open-Access, Double-Blind, Peer-Reviewed, Refereed, Multidisciplinary Online Journal
ISSN: 2581-9429
Volume 5, Issue 8, April 2025
Impact Factor: 7.67

European Journal of Engineering and Technology Research, 9(1), 10–15. https://doi.org/10.24018/EJENG.2024.9.1.3118.

[11] Zervos, M., Othonos, A., Tanasă, E., &Vasile, E. (2019). High-Temperature Pb Doping of SnO2 and Growth Limitations of PbxSn1- xO2 Nanowires Versus Low-Temperature Growth of PbxSn1- xO for Energy Storage and Conversion. Journal of Physical Chemistry C, 123(26), 16415–16423. https://doi.org/10.1021/ACS.JPCC.9B02865

[12] Sun, Q. C., Yadgarov, L., Rosentsveig, R., Seifert, G., Tenne, R., &Musfeldt, J. L. (2013). Observation of a burstein-moss shift in rhenium-doped MoS2 nanoparticles. ACS Nano, 7(4), 3506–3511. https://doi.org/10.1021/NN400464G